Ag_3PO_4/ZnO nanostructured composites fabricated through electrospun and co-mixing methods with enhanced photocatalytic activities

XINGGUANG WANG[a,b], BIAO ZHANG[a], MINGMING LI[a], YANG ZHAO[a,*], HUAN WANG[a,**], HUAIYUAN WANG[a]
[a]*College of Chemistry and Chemical Engineering, Northeast Petroleum University, Daqing, 163318, PR China*
[b]*Shandong Sinocera Functional Material CO., LTD, No. 24, Liaohe Road, Dongying, Shandong Province, PR China*

The novel Ag_3PO_4/ZnO nanocomposite photocatalyst was fabricated by the combination of electrospun and co-mixing methods. The surface morphologies, structures, compositions, chemical states and optical properties of photocatalysts were characterized by scanning electron microscope (SEM), X-ray diffraction (XRD), UV-vis diffuse reflectance spectra (DRS) and X-ray photoelectron spectroscopy (XPS), respectively. When the mass ratio of Ag_3PO_4 to ZnO was controlled to 5:8, the composite photocatalyst exhibited the best performance by the decomposition of rhodamine B (Rh-B) dye under visible light. The enhanced photocatalytic activities can be ascribed to the synergistic effect between Ag_3PO_4 and ZnO, and a possible Z-scheme mechanism was demonstrated.

(Received February 28, 2018; accepted August 16, 2021)

Keywords: Ag_3PO_4, ZnO, Nanocomposite photocatalyst, Z-scheme mechanism

1. Introduction

Recently, environmental pollution and energy shortage have attracted excellent concerns, which has aroused great research interest in seeking out a novel efficient energy conversion technique to replace traditional fossil fuels and treat wastewater. Because wastewater discharged by industrial factory, has caused various diseases such as hypertension and respiratory disorders. Photocatalytic technology, as a promising solution, has aroused extensive attention because it can utilize solar energy to decompose contaminants in wastewater.

Semiconductor photocatalysts, such as TiO_2 [1], CuO [2], NiO [3, 4], WO_3 [5], has been arousing a variety of research interest in the field of photocatalysis. Zinc oxide (ZnO), as an important wurtzite structural direct bandgap semiconductor, has been obtaining wide application including UV sensors or lasers [6], dye sensitized solar cells [7-9], gas sensors [10-12], UV lasers [13, 14] and so on. Benefiting from its excellent photoelectronic properties with a wide direct band gap of 3.37 eV and a large excitation binding energy of 60 meV [15], ZnO is suitable as photocatalyst to treat wastewater by absorbing high-energy UV photons. However, its photocatalytic performance was limited by low quantum efficiency resulted from rapid electron-hole pair recombination and inefficient utilization.

Many efforts have been devoted to enhance the photoelectrochemical efficiency, including doping noble metals or non-metals, coupling ZnO with other semiconductors. Ag_3PO_4 as the semiconductor material with a narrow bandgap of 2.45 eV, have been considered for visible-light response. Early in 2010, Yi et al. reported Ag_3PO_4 can harness visible light to oxidize water as well as decompose organic contaminants in aqueous solution [16]. After that, Ag_3PO_4 has attracted considerable attention as a potential visible light photocatalyst in the field of photocatalysis.

Nanoscale photocatalyst has been widely investigated due to its unique properties such as large surface-to-volume ratio, quantum effect, superparamagnetism, and electronic effects [17-23]. Electrospun is a simple and versatile technique, by which we can modulate hierarchical features such as nonwoven, aligned or patterned fibers, nanoribbons, nanorods and random 3D structures [24-26].

In this work, we successfully prepared Ag_3PO_4/ZnO composites through a combination of electrospun technique and co-mixing methods. The as-prepared Ag_3PO_4/ZnO exhibited considerably enhanced photocatalytic activity of decomposition of rhodamine B (Rh-B) dye under visible light. A possible Z-scheme photocatalytic mechanism was discussed about the synergistic effect between Ag_3PO_4 and ZnO in the decomposing Rh-B process.

2. Experimental

Materials: Zinc acetate dihydrate ($Zn(Ac)_2 \cdot 2H_2O$), ethanol and N, N-dimethylformamide (DMF) were purchased from Tianjin Damao chemical regent factory. Silver nitrate ($AgNO_3$), Sodium phosphate dibasic (Na_2HPO_4) and polyvinyl pyrrolidone (PVP, $M_W \approx 1300000$) were supplied by Aladdin (Shanghai, China). Rhodamine B (Rh-B) was obtained from Sigma-Aldrich. All chemicals were analytical grade and used without further purification.

2.1. Fabrication of nanoparticle ZnO

A mixture of ZnO sol-gel solution was prepared. Typically, 0.63 g $Zn(Ac)_2 \cdot 2H_2O$ were dispersed in the mixing solution of ethanol and DMF (volume ratio = 3:1) for 3 h at room temperature. After that, 1.12 g PVP was slowly added into the mixed solution with strongly stirring and stirred for 10 h to obtain a fine suspensious solution as the precursor using electrospun process.

For electrospun, the suspensious solution was added into a 20 mL plastic syringe and placed in a syringe pump. The positive voltage of 15 kV was applied between the needle and collector to form high voltage electric field, and the distance between needle and collector was 15 cm. The feeding rate of the solution was 0.5 mL/h and a Tylor cone arose in the top of needle. A white membrane could be obtained in collector, subsequently. The obtained white membrane was dried at 60 °C for 6 hours to removal resultant solvent, then heated to 550 °C for 2h at heated rate of 10 °C/min. Finally, the ZnO nanoparticles was obtained.

2.2. Fabrication of Ag_3PO_4/ZnO composite

160 mg ZnO nanoparticles was dispersed in 200 mL deionized water and stirred for 30 min to form solution 1. Then, 20 mg $AgNO_3$ was added to 30 mL of deionized water to form solution 2 and was added to solution 1 with strong stirring. After that, 10 mL of Na_2HPO_4 solution (0.02 M) were dropwise adding the above mixing solution and stirring for 10 h. The solids were filtered and then washed several times with distilled water and ethanol. Finally, the as-prepared samples were dried in air at 70 °C over night and the Ag_3PO_4/ZnO composite with the mass ratio of 1:8 of Ag_3PO_4 to ZnO denoted as AZ1. Further composites were prepared with the mass ratio of Ag_3PO_4/ZnO was controlled to 3:8, 5:8, 7:8 and 9:8, denoted as AZ2, AZ3, AZ4, AZ5, respectively.

2.3. Characterization

The morphologies of the as-prepared composites were observed a Zeiss Sigma scanning electron microscope (SEM) (Zeiss Sigma). X-ray diffraction (XRD) of composites were collected using a Rigaku D/MAX 2200 diffractometer with Cu Kα radiation (λ= 0.15406 nm). The X-ray photoelectron spectroscopy (XPS) was performed using X-ray photoelectron spectrometer (AXIS ULTRA DLD, Shimadzu, Japan). The UV-vis diffuse reflectance spectroscopy (DRS) was measured using a Shimadzu UV-2550 UV-vis spectrometer employing barium sulfate as white standard. The UV-Absorption spectra of Rh-B were measured employing UV-vis spectrophotometer (MAKPADA UV-1600 Shanghai, China).

2.4. Evaluation of photocatalytic performance

The photocatalytic activity of as-synthesized composites was investigated by the degradation of Rh-B solution under visible-light irradiation. Briefly, 50 mg of each of photocatalyst were dispersed into 50 mL Rh-B aqueous solution (1.0×10^{-5} mol/L) in a beaker. Prior to irradiation, the suspensions were magnetically stirred in the dark for 30 min to obtain adsorption-desorption equilibrium between Rh-B and the catalyst surface, then the light irradiation was carried out using 300 W Xe lamp with a super cold filter. During illustration, 3 mL suspension was taken out at 15 min time interval and separated the nanoparticles from the solution by centrifugation process. The centrifuged solution was measured on a UV-vis spectrophotometer and recorded the decrease in absorbance at 553 nm.

3. Results and discussion

The morphologies of pristine ZnO and Ag_3PO_4/ZnO composites were characterized by SEM. Fig. 1a shows the spatial interlaced three-dimensional structure of ZnO prepared by the electrospun. From the partial magnified area, it can be seen that the ZnO nanoparticles are constituted to above structure. The morphology of nanoparticles further dispersed by the stirring is shown in Fig. 1b. Fig. 1c shows the morphology of a certain amount of Ag_3PO_4 mixed with ZnO to form AZ3. After the heating treatment, the ZnO nanoparticles were loaded on the surface of Ag3PO4 agglomerations (Fig. 1d).

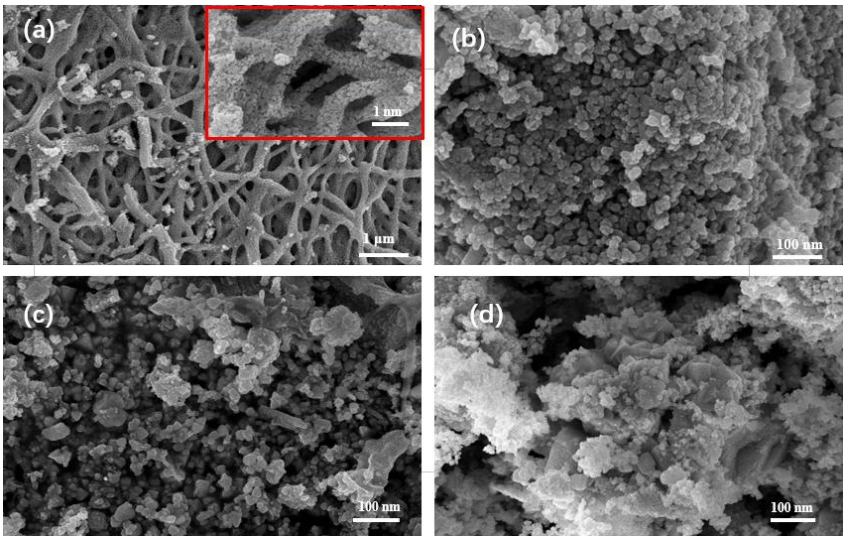

Fig. 1. SEM images of three-dimension ZnO (a), ZnO nanoparticles (b) and Ag_3PO_4/ZnO composite (c, d)

Fig. 2 shows the XRD patterns of the Ag_3PO_4/ZnO composites, ZnO and Ag_3PO_4. The diffraction peaks of ZnO were observed at 2θ = 31.7°, 34.4°, 36.3°, 47.5°, 56.6°, 62.9°, 67.9°, 69.0°, 72.7° and 76.89°, which are indexed at diffraction lines of (110), (002), (101), (101), (102), (110), (103), (112), (201), (004) and (202). All the peak positions are in good agreement with the JCPDS file of ZnO (JCPDS no: 01-1136). In addition, the diffraction peaks of Ag_3PO_4 were observed at 2θ = 20.8°, 29.7°, 33.3°, 36.5°, 47.7°, 52.6°, 55.0°, 61.6° and 71.8°, which are indexed at diffraction lines of (110), (200), (210), (211), (310), (222), (320), (321), (400) and (421). Furthermore, the XRD patterns revealed that the as-synthesized Ag_3PO_4/ZnO composite materials consist of both ZnO and Ag_3PO_4 phases, and the Ag_3PO_4 peak intensities increase gradually with increasing the content of Ag_3PO_4 in the composite. The XRD patterns confirmed the formation of as-synthesized Ag_3PO_4/ZnO composite materials.

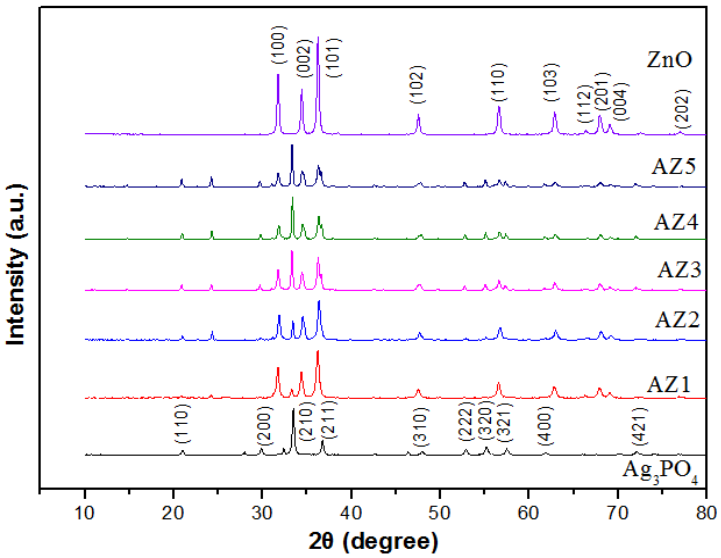

Fig. 2. XRD patterns of Ag_3PO_4, Ag_3PO_4/ZnO composites and ZnO (color online)

X-ray photoelectron spectroscopy (XPS) is a quantitative spectroscopic method used to determine the compositions and chemical-states of the elements existed in the materials. From the full XPS spectrum of the sample in Fig. 3a, the chemical states of Zn, Ag, O and P can be observed. As shown in Fig. 3b, the peaks located at 1021.8 and 1044.9 eV, corresponding to the Zn 2p1/2 and Zn 2p 3/2 of ZnO, respectively, suggesting a normal state Zn^{2+} in Ag_3PO_4/ZnO composite [27]. In Fig. 3c, the Ag 3d peak of Ag_3PO_4/ZnO composite was composed of the Ag^+ and Ag^0 peak. The strong peaks at ~374 and ~368 eV, which can be attributed to Ag^+ d3/2 and Ag^+ d5/2 levels, respectively. While the weak peaks at 374.3 and 368.4 eV belong to metal Ag^0, which revealed that a minute quantities of

metallic Ag in composite [28]. For the O 1s, the binding energy of ca. 530 eV is assigned to O^{2-} anion in Fig. 3d. This further verifies the states of elemental as-prepared composites.

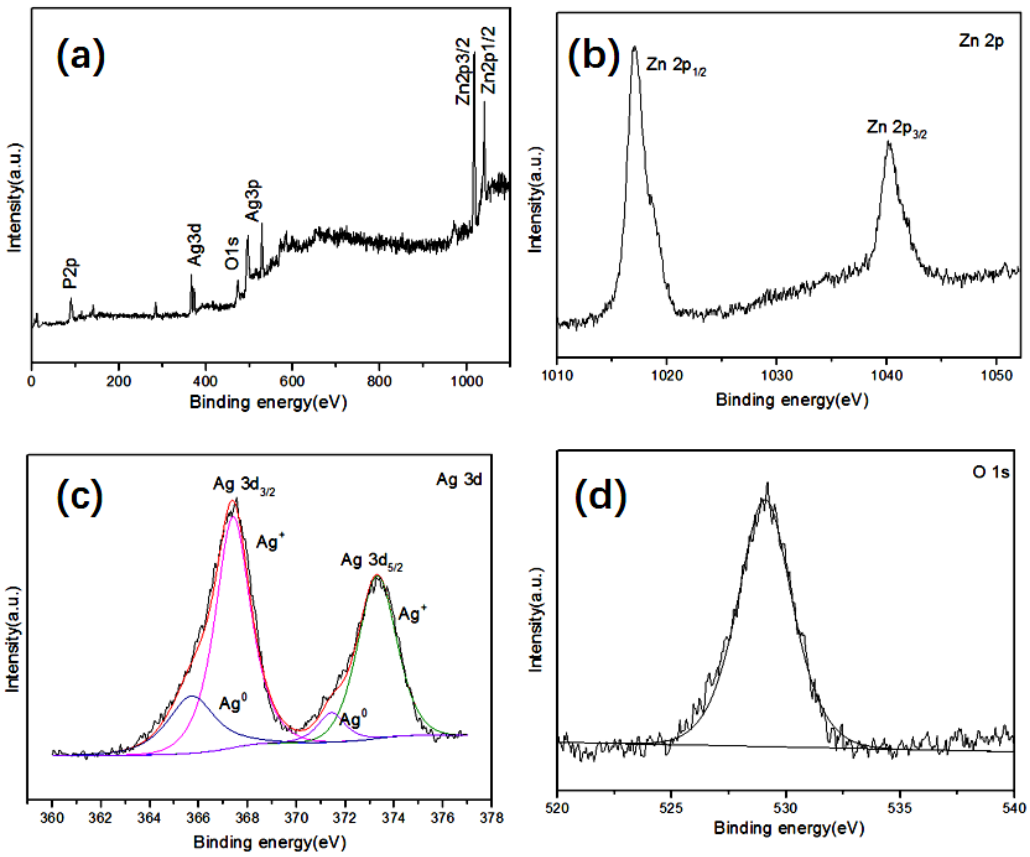

Fig. 3. XPS full length spectrum(a), the spectrum of Zn 2p (b), Ag 3d (c) and O 1s (d) (color online)

The UV-vis diffused reflectance spectra of the prepared ZnO, Ag_3PO_4/ZnO composites and Ag_3PO_4 are shown in Fig. 4. A sharp basal absorption of edge for ZnO at 415 nm, corresponding to a band gap estimated at 2.99 eV. After doping of Ag_3PO_4, it can be observed that the absorption edge of Ag_3PO_4/ZnO composite moved from 431 nm to 489 nm, which is corresponded with the band gap shift from 2.88 to 2.54 eV. The result exhibited that doping of Ag_3PO_4 make the absorption edges of Ag_3PO_4/ZnO composites extend to the lower energy religion, which is ascribed to the formation of strong chemical bonds between Ag_3PO_4 and ZnO.

The photocatalytic activities of AZ composites were measured by degrading organic pollutants Rh-B under the irradiation of visible light. The degradation efficiency of the photocatalyst for Rh-B dye is calculated as: C / C_0, where C_0 is the original concentration of aqueous Rh-B dye and C is the concentration of Rh-B with photocatalyst following light exposure intervals. Fig. 5a showed the UV-visible absorption spectra for AZ3 under visible light. Obviously, it can be seen that the maximum absorption peak strikingly reduced after 15 min under light irradiation, and completely disappeared after 90 min of irradiation. It is noted that the maximum absorption peak shift to the lower wavelength region (hypsochromic shift) with the increasing in the irradiation time, which can be ascribed to the formation of the intermediates during the process of Rh-B disintegration. Moreover, all photocatalytic activity of AZ-composites was displayed as a function between the efficiency of the photocatalysts degradation and intervals time, shown in Fig. 5b. It is can be seen that all the Ag_3PO_4/ZnO composites displayed higher photocatalytic efficiency than that of pure ZnO and Ag_3PO_4. Among all the Ag_3PO_4/ZnO composites, the AZ3 exhibited the maximum photocatalytic efficiency. Whereas, with the content of Ag_3PO_4 further increasing, it is can be observed that the photocatalytic efficiency presents a certainly slight decrease, which can be ascribed to the transportation of photo-generated electrons from Ag_3PO_4 to ZnO is blocked.

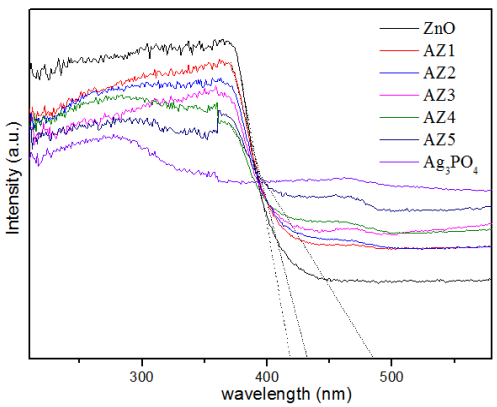

Fig. 4. UV–vis diffuse reflectance spectra of ZnO, Ag_3PO_4 and the Ag_3PO_4/ZnO composites (color online)

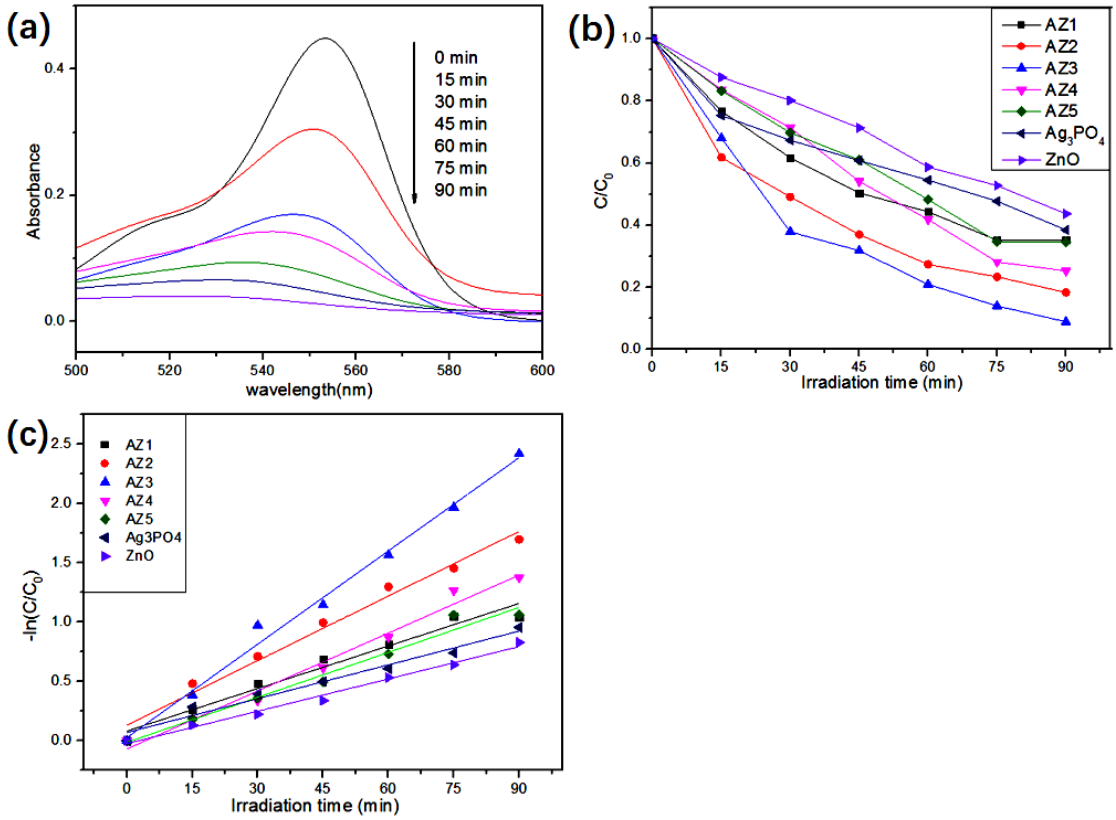

Fig. 5. UV-Absorption spectra (a), degradation rate (b) and first-order rate constant (c) of Ag_3PO_4/ZnO composites on degradation of Rh-B (color online)

In order to display better comparison of the photocatalytic efficiency rate of different AZ photocatalysts under visible irradiation, the kinetic simulation of the degradation of Rh-B over the above photocatalysts was demonstrated. As is shown in Fig. 5c, all experimental data were plotted as linear curves, following a Langmuir-Hinshelwood pseudo first-order kinetics model:

$$\ln(c/c_0) = -k_{app}t \quad (1)$$

where, C/C_0 is the same meaning as above degradation efficiency of Rh-B; k_{app} is the reaction rate constant (min^{-1}); t is the irradiation time. In Fig. 5c, the maximum reaction rate constant of the Rh-B degradation is the 0.0262 min^{-1} for AZ3, which is about 3 times higher than that of pure ZnO (0.0091 min^{-1}) and 2.7 times higher than that of pure Ag_3PO_4 (0.0095 min^{-1}). Therefore, AZ3, as an optimum content of Ag_3PO_4 in composite, exhibited a better photocatalytic activity than ZnO and Ag_3PO_4, which can be ascribed to the synergistic effect between ZnO and Ag_3PO_4.

To better illustrate the above results, a possible Z-scheme mechanism for Ag_3PO_4/ZnO composites was given in Fig. 6. When the photocatalyst is exposed to light irradiation, the photoinduced electron-hole pairs are produced. Then the electrons in the conduction band (CB) of Ag_3PO_4 transferred to the valence band (VB) of ZnO, recombining the holes in the valence band (VB) of ZnO. As a result, the photo-generated electrons and holes can be maintained in ZnO and Ag_3PO_4 respectively, which ensure superior oxidation and reduction ability of the photocatalysts in the same time. The improved performance of the photocatalyst was mainly ascribed to the direct Z-scheme mechanism between ZnO and Ag_3PO_4, which benefit the migration and separation of photoinduced electron-hole pairs and enhance the photocatalytic ability of ZnO and Ag_3PO_4.

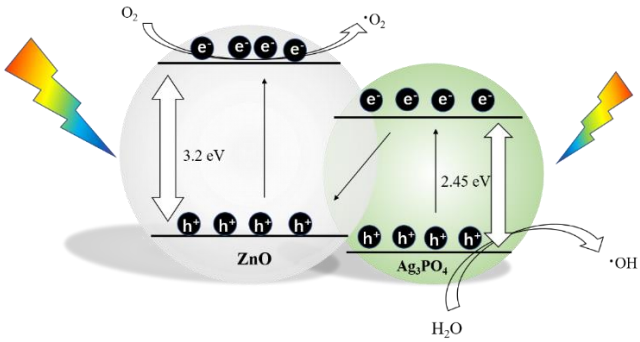

Fig. 6. Z-scheme schematic diagram of Ag_3PO_4/ZnO composite (color online)

4. Conclusion

In this work, the Ag_3PO_4/ZnO nanomaterial was prepared through combination of electrospun and co-mixing methods. The material was characterized by SEM, XRD, XPS, and DRS. The Ag_3PO_4/ZnO exhibited enhanced photocatalytic activity. Our experiment shows that the photodecomposition efficiency of Rh-B under 300 W of visible light by photocatalysis AZ3 is better than that of other photocatalysts. The improvement of photocatalytic activity is mainly ascribed to direct contact and synergistic effect between Ag_3PO_4 and ZnO. Photoinduced electron-hole pairs can be effectively separated at the interface that is believed to another factor for boosting the photocatalytic activity of photocatalyst. The results point out Ag_3PO_4 hybrid semiconductors photocatalyst give a facile and promising route for pollutants decomposition.

Acknowledgements

We are grateful for financial support from the China Postdoctoral Science Foundation (2021M693793, 2019T120251, 2018M630334), Natural Science Foundation of Heilongjiang Province (YQ2019E009), Heilongjiang Postdoctoral Young Talent Program (LBH-TZ05), Heilongjiang Postdoctoral Scientific Research Developmental Fund (LBH-Q17034), University Nursing Program for Young Scholars with Creative Talents in Heilongjiang Province (UNPYSCT-2020143), and Heilongjiang Postdoctoral General Fund (LBH-Z20123).

References

[1] J. Schneider, M. Matsuoka, M. Takeuchi, Chem. Rev. **114**(19), 9919 (2014).
[2] L. Zhang, Z. Gao, C. Liu, RSC Adv. **4**(88), 47455 (2014).
[3] S. G. Hosseini, R. Abazari, RSC Adv. **5**(117), 96777 (2015).
[4] F. Fazlali, A. R. Mahjoub, R. Abazari, Solid State Sci. **48**, 263 (2015).
[5] K. Jothivenkatachalam, S. Prabhu, A. Nithya, RSC Adv. **4**(41), 21221 (2014).
[6] H. Dong, Y. Liu, J. Lu, J. Mater. Chem. C **1**(2), 202 (2013).
[7] D. Sengupta, P. Das, B. Mondal, Renew Sust. Energ. Rev. **60**, 356 (2016).
[8] L. De Marco, D. Calestani, A. Qualtieri, Sol. Energ. Mat. Sol. C. **168**, 227 (2017).
[9] B. Siwach, S. Sharma, D. Mohan, J. Integ. Sci. Technol. **5**(1), 1 (2017).
[10] E. Dilonardo, M. Alvisi, G. Cassano, MRS Adv. **2**(18), 1001 (2017).
[11] B. Wu, Z. Lin, M. Sheng, Appl. Surf. Sci. **360**, 652 (2016).
[12] V. Galstyan, E. Comini, I. Kholmanov, RSC Adv. **6**(41), 34225 (2016).
[13] C. Cheng, R. Lin, H. Lin, J. Laser Micro. Nanoen. **11**(1), 13 (2016).
[14] G. Zhu, Int. J. Nanotechnol. **2017**, 1 (2017).
[15] Y. Zheng, C. Chen, Y. Zhan, Inorg. Chem. **46**(16), 6675 (2007).
[16] Z. Yi, J. Ye, N. Kikugawa, Nat. Mater. **9**(7), 559 (2010).
[17] C. P. Bean, J. D. Livingston, J. Appl. Phys. **30**(4), S120 (1959).
[18] M.-C. Daniel, D. Astruc, Chem. Rev. **104**(1), 293 (2004).
[19] J. Li, S. Wang, G. Sun, Mater. Today Chem. **19**, 100390 (2021).
[20] T. Cheng, H. Gao, X. Sun, Adv. Powder Technol. **32**(3), 951 (2021).
[21] Y. Wang, R. Li, X. Sun, J. Electron. Mater. **50**, 2674 (2021).
[22] T. Cheng, X. Sun, T. Xian, Opt. Mater. **112**, 110781 (2021).
[23] Y. Xu, Q. Cao, Z. Yi, IEEE Access. **8**, 171350 (2020).
[24] S. Cavaliere, S. Subianto, I. Savych, Energ. Environ. Sci. **4**(12), 4761 (2011).
[25] L. S. Carnell, E. J. Siochi, R. A. Wincheski, Scripta Mater. **60**(6), 359 (2009).
[26] Q. Yu, M. Wang, H. Chen, Mater. Lett. **64**(3), 428 (2010).
[27] Z. Zhang, C. Shao, X. Li, ACS Appl. Mater. Inter. **2**(10), 2915 (2010).
[28] C. Tang, E. Liu, J. Wan, Appl. Catal. B-Environ. **181**, 707 (2016).

Corresponding author: fredericagreenhill@163.com
wanghuan83214@gmail.com**